Title

Geometry of Charge Density as a Reporter on the Role of the Protein Scaffold in Enzymatic Catalysis: Electrostatic Preorganization and Beyond

Journal

Journal of Chemical Theory and Computation, 19(3)

ISSN

1549-9618

Authors

Eberhart, Mark E
Wilson, Timothy R
Johnston, Nathaniel W
et al.

Publication Date

2023-02-14

DOI

10.1021/acs.jctc.2c01060

Peer reviewed

Geometry of charge density as a reporter on the role of protein scaffold in enzymatic catalysis: electrostatic preorganization and beyond

Mark E. Eberhart,[a*] Timothy R. Wilson,[1] Nathaniel Johnston,[2] and Anastassia N. Alexandrova[b+]

[1]*Department of Chemistry, Colorado School of Mines, Golden, Colorado 80401, USA*
[2]*Department of Chemistry, and Biochemistry, University of California, Los Angeles, Los Angeles, California 90095, USA*

Abstract: Enzymes host active sites inside protein macromolecules, which have diverse, often incredibly complex, and atom-expensive structures. It is an outstanding question what the role of these expensive scaffolds might be in enzymatic catalysis. Answering this question is essential to both enzymology and the design of artificial enzymes with proficiencies that will match those of the best natural enzymes. Protein rigidifying the active site, contrasted with the dynamics and vibrational motion promoting the reaction, as well as long-range electrostatics (also known as electrostatic preorganization) were all proposed as central contributions of the scaffold to the catalysis. Here, we show that all these effects inevitably produce the changes in the quantum mechanical electron density in the active site, which in turn defines the reactivity. The phenomena are therefore fundamentally inseparable. The geometry of the electron density – a scalar field characterized by a number of mathematical features such as critical points – is a rigorous and convenient descriptor of enzymatic catalysis, and a reporter on the role of the protein. We show how this geometry can be analyzed, linked to the reaction barriers, and report in particular on intramolecular electric fields in enzymes. We illustrate these tools on the studies of electrostatic preorganization in several representative enzyme classes, both natural and artificial. We highlight the forward-looking aspects of the approach.

TOC Graphics:

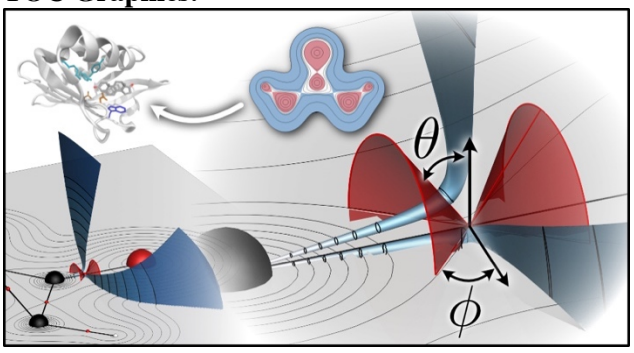

1. Introduction

Electrostatic preorganization (EP), the arrangement of charged groups in enzymes to electrostatically favor the transition state over the reactants, was proposed by Warshel to be a driving force in enzymatic catalysis.[1,2] For a reaction to occur in solvent, the solvent must rearrange to lower the enthalpy of the transition state, whereas proteins avoid this rearrangement through preorganization. Thus, reactions in

[a] Department of Chemistry, Colorado School of Mines, 1500 Illinois St., Golden, CO 80004, USA
[*] email: meberhar@mines.edu
[b] Department of Chemistry, UCLA, 607 Charles E. Young Drive East, Los Angeles, CA 90095, USA
[+] email: ana@chem.ucla.edu

solvent incur an entropy cost that proteins avoid, allowing enzymatic reactions to have a lower free energy barrier. This hypothesis was confirmed in experiments by Boxer, which have driven significant recent interest in EP. Boxer has used vibrational Stark effect (VSE) spectroscopy, which uses the shift in vibrational frequencies of a reporter molecule to measure local electric fields, to report on electric fields in the active sites of various enzymes.[3,4] The Boxer group found that ~70% of ketosteroid isomerase's catalytic effect is due to the active site electric field.[5,6] Using a mix of VSE spectroscopy and MD simulations, they also found that the selectivity of TEM β-lactamases depends on both the electric field in the active site and on positioning of chemically relevant residues.[7] Thus, both theoretical and experimental work have found significant evidence for the importance of EP in enzymatic catalysis. However, to date, it is not entirely clear whether EP is always at play in enzymes.

At the same time, the role of mid- and long-range electrostatics as the main contribution of the protein scaffold to catalysis is vigorously challenged. Perhaps the most prominent competing theory capitalizes on the role of protein promoting vibrations (PPVs). PPVs occur on the timescale of an individual barrier crossing event (hundreds of femtoseconds), in between the timescales of individual bond vibrations and large conformational changes.[8] These vibrations are hypothesized by Schwartz and colleagues to cause compression of the active site along the reaction coordinate, lowering the reaction barrier in the enzyme.[9,10] PPVs have been investigated computationally via molecular dynamics and transition path sampling and experimentally via heavy atom substitution, and they have been implicated in the catalytic activity of enzymes such as purine nucleoside phosphorylase[11–13] and lactate dehydrogenase.[9,14] Notably, promoting vibrations are absent in *E. coli* dihydrofolate reductase, indicating that PPVs alone cannot explain all of enzymatic catalysis.[15,16] There is clearly a need for other methods of interrogating catalytic mechanisms in proteins.

Theory is quite central at elucidating the various roles that the protein plays, and indeed much of the debate is among theorists. Theoretically detecting EP has been done via computational Stark spectroscopy,[17,18] polarizable force fields,[19,20] and empirical valence bond (EVB) calculations.[1,21,22] Dynamics studies on the other hand often focus on protein rigidity[23] or PPVs. Some computational studies have found changes in the active site electric field due to protein dynamics,[18,24,25] but the importance of preorganization vs. dynamics remains contested. Hence, theorists cannot quite agree, and experimentalists are short of tools. We believe the dissonance in the field has a solution.

In this article we discuss an alternative approach to detecting the contributions of the protein scaffold in enzymatic catalysis, which is based on the geometry of the quantum mechanical electron density in the active site. We will show that this can serve as a highly sensitive and sophisticated probe for varying protein electrostatics. Additionally, since the electron density is dependent on the molecular geometry of the active site and its surroundings, our method reports on the relationship between electrostatic effects and configurational perturbations. Thus, we are able to unify the previously conflicting theories of electrostatic preorganization and protein promoting vibrations.

2. Background

2.1. QTAIM

Our approach builds on the Quantum Theory of Atoms in Molecules.[26–30] This theory derives its validity from two independent observations. First, that the charge density, $\rho(\boldsymbol{r})$, possesses a unique topology that can be fully characterized by the type and location of the charge density extrema—maxima, minima, and saddle points—called critical points (CPs; such that $\boldsymbol{\nabla\rho}(\boldsymbol{r}_c) = 0$). There are four type of extremal points distinguished by the sign of the principal curvatures of the charge density at these points, *i.e.* the principal components the charge density Hessian ($\nabla^2\rho(\boldsymbol{r})$). At a maximum, all three principal curvatures

are positive, and as these occur most frequently at nuclear sites, they are called nuclear critical points (NCP). At a charge density minimum, all three principal curvatures are negative. These are called cage critical points (CCP). Then there are two type of saddle points, one called a bond critical point (BCP), where two principal curvatures are negative and the other is positive, and another called a ring critical point (RCP) with two positive and one negative principal curvature. CPs are characterized by such mathematical descriptors as the charge density Laplacian at the CP, the electrostatic potential, the Lagrangian electronic kinetic energy density, and the delocalization index in the bond (δ(A,B)).

The second observation intrinsic to the validity of QTAIM is that while local electronic kinetic energy and hence local total energy is ambiguous, over specific volumes the integrated kinetic energy is well defined. Together these observations allow one to identify topologically distinct volumes surrounding atomic nuclei possessing well-defined energies and other atomic properties such as electron counts. These regions are called atomic basins that are defined by zero-flux surfaces, *i.e.* surfaces whose normal vector at any point, $\boldsymbol{n}(\boldsymbol{r})$, satisfies $\boldsymbol{\nabla\rho}(\boldsymbol{r}) \cdot n(\boldsymbol{r}) = 0$. Atomic basins have been identified as the "atoms in molecules."

2.2. Applications to Enzyme Catalysis

Our initial application involving QTAIM revolved around efforts to correlate catalytic activity with local parameters, such as interatomic distances, values of ρ and its derivatives at molecular critical points (CPs) and atomic basin properties. It was hoped that such data could be rapidly "mined" and used in statistical models to screen new systems and predict their relative catalytic activities.

As an example, the pioneering investigation of Morgenstern *et al*.[31] sought to quantify the effects of EP by stepwise increasing the active site model of Histone Deacetylase 8 (HDAC8) to include more distant amino acid residues. The investigators found that the magnitude of charge density at CPs and most Bader atomic charges converged quickly as more of the protein was included in the simulation. The exact position of critical points, however, was found to converge more slowly and to be strongly influenced by the protein residues that are further from the active site. It was argued that the positions of critical points were affected through perturbations to the wavefunctions in the active site caused by dipole moments from amino acid residues throughout the protein and that the fingerprint of CP, from the point of view of charge density, could not be easily understood through the charges on atoms or the nature of the bonding interactions, but through the relative positions of CPs known to correlate with reactivity and reaction barriers.

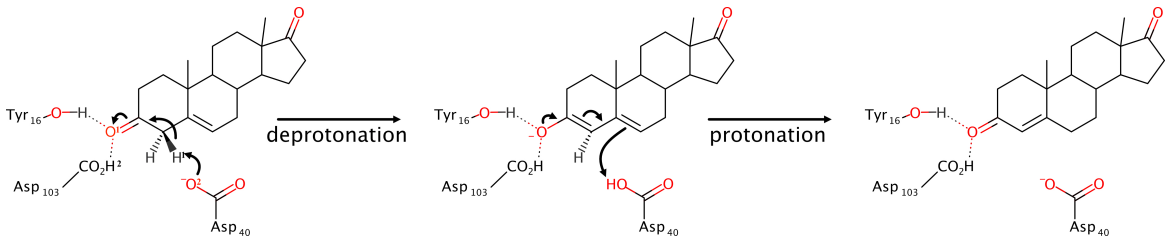

Scheme 1. Steroid isomerization reaction catalyzed by KSI.

Furthermore, this study showed that the changes in the charge density in the active site upon reaction barrier crossing can be viewed as a reaction coordinate in ρ. Note that this reaction coordinate does not need to coincide with the motion of the atomic nuclei. Specifically, in HDAC8 (Figure 1), the region of the active site defined by the catalytic Zn^{2+} cation, the activated carbonyl of the substrate (C1=O1) bound to that Zn^{2+}, and the O atom of the nucleophilic water molecule (Ow), contains the reaction coordinate for the nucleophilic attack, which can be detected with a naked eye (which is probably not the case for all other reactions). The region is bounded by 4 bond paths, each characterized by its BCP. It is therefore geometrically required that there would be a RCP in the center of that region. As the nucleophilic attack takes place, the C1=Ow bond forms, and the Zn-Ow bond breaks (Zn-Ow BCP disappears). During the barrier crossing, the most obvious motion in ρ corresponds to the RCP and the Zn-Ow BCP approach each other and mutually annihilate. Thus, the distance between these CPs (red arrow in Figure 1 right) can be viewed as a reaction coordinate in ρ. Note that this view is rather simplified because the entire charge density undergoes a perturbation, with multiple regions responding to the barrier crossing (consider, *e.g.*, the obvious C1=O1 bond, and the Bader charge on the C1 atom). We will go in more details about the global geometric response of ρ to chemical and physical perturbations later in the article. For now, suffice it to say that the reactant state ρ clearly contains descriptors of the reactivity in enzymes (and not only in enzymes).

These results served to partially motivate QTAIM related investigations exploring electrostatic preorganization of the well-studied steroid isomerization reaction catalyzed by ketosteroid isomerase (KSI) that involves the repositioning of a double C=C bond in the steroid substrate.[32–35] As shown in Scheme 1, this occurs by the removal of a proton from the secondary β-carbon, which is redeposited at the adjacent secondary carbon.

Fuller *et al*. considered the effects of applied external electric fields (EEFs) to this process using the small-scale KSI active site model and found that a field applied parallel to the substrate carbonyl bond,

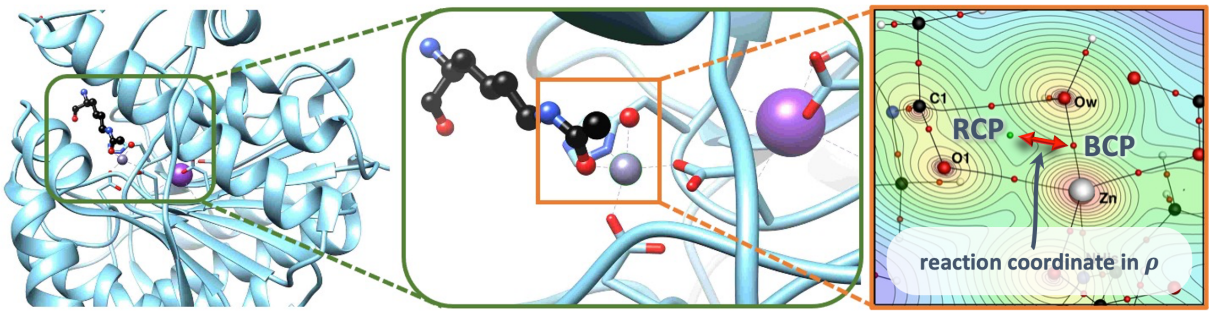

Figure 1. Histone deacetylase, HDAC8, its active site with the bound substrate and the nucleophilic water activated by Zn, and the QTAIM ρ of the area, showing important CPs and the reaction coordinate in ρ (*vide infra*). Right: small red and green spheres represent bond and ring CPs respectively.

pointing from O to C lowered the reaction barrier, while a field in the opposite direction raised it.[36] Correlations between these changes to the reaction barrier due to the applied EEFs and several local properties were sought. The strongest correlation found was that of the bond length of the H1—O2 interatomic distance, which correlated positively with the change in reaction barrier, while the value of ρ at the corresponding bond CP anti-correlated. A weaker positive correlation was found with H2—O1 interatomic distance (Figure 2).

Hennefarth and Alexandrova subsequently demonstrated similar reaction barrier effects in KSI variants that had a tyrosine mutated to a 3-chlorotyrosine.[35] To identify the features responsible, they conducted a regional electric field curvature analysis within two separate rectilinear volumes, one containing the carbonyl C=O1 atoms, and the other containing the C—H1···O2 atoms of the reaction site. By evaluating the total curvature along $\boldsymbol{E}(\boldsymbol{r})$ streamlines within each volume, they generated histograms that reflect the relative occupations of high and low curvature regions. The corresponding volumes of multiple systems could then be compared by computing the corresponding histogram distances, thus providing a scalar pairwise "similarity metric." They then compared the similarity between corresponding regions in each pair of systems to changes in reaction barrier height in order to correlate $\boldsymbol{E}(\boldsymbol{r})$ curvature with catalytic activity.

Using this approach, Hennefarth and Alexandrova found that the $\boldsymbol{E}(\boldsymbol{r})$ curvature about the carbonyl bond had a stronger correlation with reaction barrier than that of the reaction site, with 3-chlorotyrosine mutants included in the analysis. This finding is counter to the results of local structural analyses (and those of Fuller et al.) that the strongest correlations occur in the reaction site rather than within the substrate. The regional results indicate that activation of the carbonyl enhances the reaction rate, where analyses of local structures points to a different rate determining step in the catalytic mechanism. That is, a regional approach seems to better reveal the underlying chemistry at work common to both the EEF and mutant KSI systems.[37,38]

While carbonyl activation in KSI benefits the steroid isomerization for chemically obvious reasons, there are reactions where the region of charge density whose attenuation by an electric field would affect the reaction is less obvious. One example is pericyclic reactions, such as the Diels-Alder reaction. It has been shown theoretically that applying an electric field across this reaction affects the barrier crossing.[39,40] Later, the effect was confirmed experimentally when a diene and a dienophile were placed at an STM break junction, and the field produced at the

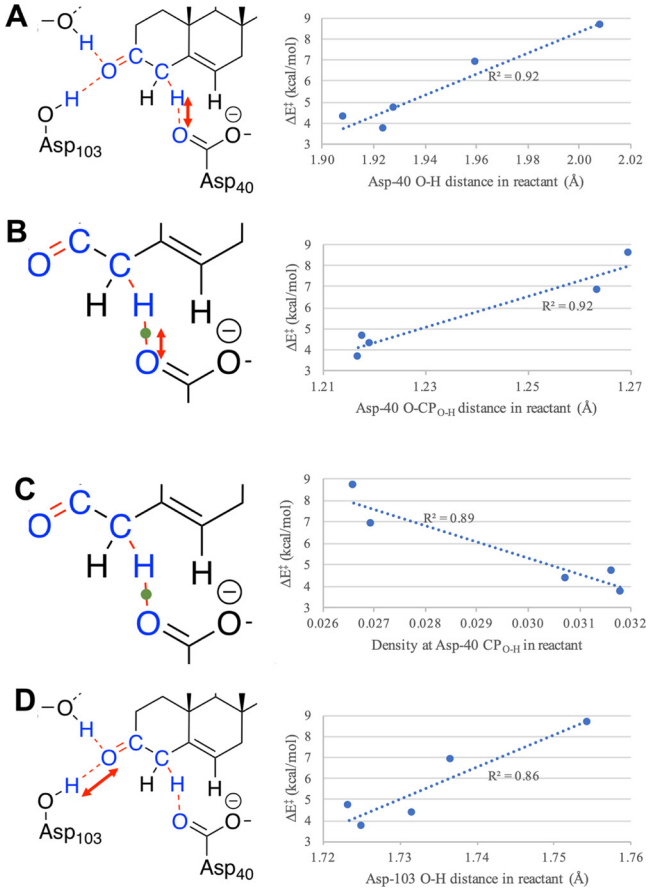

Figure 2. Geometric and QTAIM parameters found to exhibit the best correlations with the computed reaction barriers for the first step of the reaction at varying external electric fields: (A) the Asp-40 O–H distance, (B) the distance between the Asp-40 $CP_{O–H}$ and the Asp-40 O atom, (C) the charge density at the Asp-40 $CP_{O–H}$, and (D) the Asp-103 O–H distance. Reproduced with permission from Ref. 35.

junction was shown to affect the reaction rate.[41] We note the specificity of this experiment: the reagents had to be rather structurally rigid to retain the structure and mutual orientation when exposed to the field, presumably to avoid reorientation and confirmational changes. Without this, unbound reactants can reorient in strong fields, especially if any one of them contains polar groups. Note as well that enzymes are good exactly at constraining the reagents in a certain geometry when bound to the active site. For the Diels-Alder reaction, artificial enzymes have been made and optimized.[42–44] This merits a question of the ways in which the intermolecular electric fields have evolved during the enzyme optimization, and whether that contributed to the improved activity.

Hence, first, we aimed to find out which features of the geometry of ρ in the reactant complexes of the Diels-Alder reaction correlate with the reaction barrier height.[45] To make the inspection unbiased, we applied machine learning to identify the features of ρ important for the reactivity. The compiled dataset consisted of 296 Diels-Alder reactions in solution and included reactants with a diverse set of functional groups, sizes, and geometries. The set featured a range of barriers, as large as 270 kJ/mol. The input

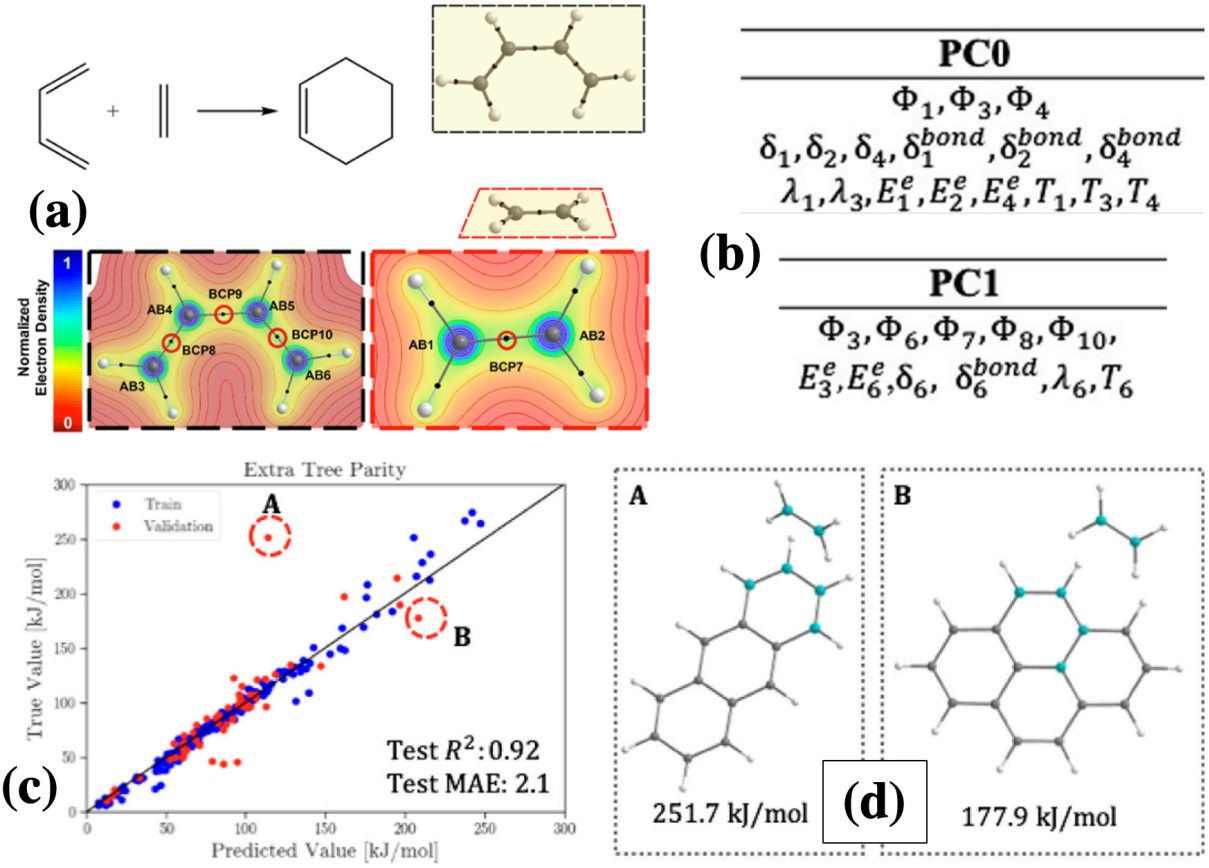

Figure 3. The Diels-Alder reaction and locations on key bond CPs (a), and PC analysis narrowing the set of descriptors of the charge density to a minimum (b), and the result of the machine learning model for the prediction of the reaction barrier from the reactant state charge density (c). The two indicated outliers A and B (c) are contain conjugated dienes and are shown in the insets (d). The full set of features before PCA included: ϵ: bond ellipticity, T: electronic energy of molecule, E^e: contribution of atom to electronic energy, q: electronic charge, σ: stress, Φ: electrostatic potential, δ: delocalization index, δ^{bond}: bond delocalization index, λ: localication index, d: average number of electronic pairs formed in atom a, d': half of average number of electron pairs formed between atom A and other atoms of molecule, d^{sum} sum of d and d'. Reproduced with permission from Ref. 45.

space for the feature selection/regression algorithms consisted of mathematical features at a fixed set of atomic basins (ABs) and CPs; we included 10 features shown in Figure 3a: 6 ABs corresponding to atoms participating in bond breaking and forming, and 4 BCPs from the dienophile and diene. From each of the 6 ABs, 9 descriptors were selected including localization/delocalization indices, electrostatic potentials, charge, and electronic energy contributions. We also include the electrostatic potential (Φ), and the electronic (Φ^e) and nuclear contributions (Φ^{nuc}), which is evaluated only at the nuclei of the AB. Note that these values are well-defined as they exclude the contribution of the nuclei. For each of the 4 BCPs, 19 descriptors were extracted including values such as ellipticity, density, stress tensor eigenvalues, density Hessian eigenvalues, divergence of density, potential energy, delocalization index, and kinetic energy (Figure 3b). Note that the parameters in this set are both rigorous and continuous – highly useful features for ML. The model showed that the electrostatic potential, Φ (including both Φ^{nuc} and Φ^e), and Bader charges (q) are the most physically important set of descriptors from a statistical standpoint. These topological descriptors of the ρ in the reactant state are predictive of reaction barriers of the Diels–Alder reaction. While we trained our single-objective supervised (labeled) regression algorithms on simpler Diels–Alder reactions in solution, they predict reaction barriers also in significantly more complicated contexts, such a Diels–Alder reaction catalyzed by an artificial enzyme and its evolved variants, in agreement with experimental changes in k_{cat}.[42,45] Finally, we also applied an external electric field to the Diels-Alder reaction in solution, and found features of ρ that faithfully predict the change in the reaction barrier under these circumstances,[37] hence yet again serving as a reporter on electrostatic preorganization (in this case set up artificially).

These investigations, while showcasing the initial success of the conventional QTAIM approaches in describing enzyme-catalyzed reactions and detecting electrostatic preorganization, also exposed their deficiencies of characterizing the charge density in terms of its topological and local descriptors, which are necessarily treated as independent parameters. ρ, however, is like a blanket; one cannot pull on one end and not affect all other parts. There is a clear need for a rationale that quantifies the global response of the charge density due to local perturbations of any sort. Our extensions to QTAIM accomplishes this goal by describing ρ in terms of the intrinsic geometry of its isosurfaces. We expect these developments to further our understanding of electrostatic preorganization as a phenomenon affecting the active site globally, and, importantly, to unify some of the ideas in the fields of enzymology and enzyme design concerning the role of the protein scaffold in promoting the reaction.

3. Geometry of the Electron Density

3.1. Isosurface and contour geometry

Electronic charge density is often represented with a set of simple closed isosurfaces that may, in turn, be pictured as contours in selected cut planes. Such representations have proved a useful way to depict a molecule's electronic response to chemical or physical perturbations. It is seldom noted, however, that in addition to chemical factors limiting this response there are geometric principles that further constrain the allowed changes to these surfaces.

The geometry of a surface about a point is determined by its two principal curvatures at that point ($\kappa_1$and κ_2). The surface's total curvature is given either by its mean curvature ($\kappa_1 + \kappa_2$) or its Gaussian curvature ($\kappa_1\kappa_2$). A point on a surface where both principal curvatures are positive is called an elliptic point, and near this point the surface is convex. If both principal curvatures are negative, the surface is said to be parabolic and is locally concave. Around a point where one principal curvature is negative and the other is positive the surface is saddle shaped and the point is called hyperbolic. Finally, about a point where at least one principal curvature vanishes, the surface is topologically flat.

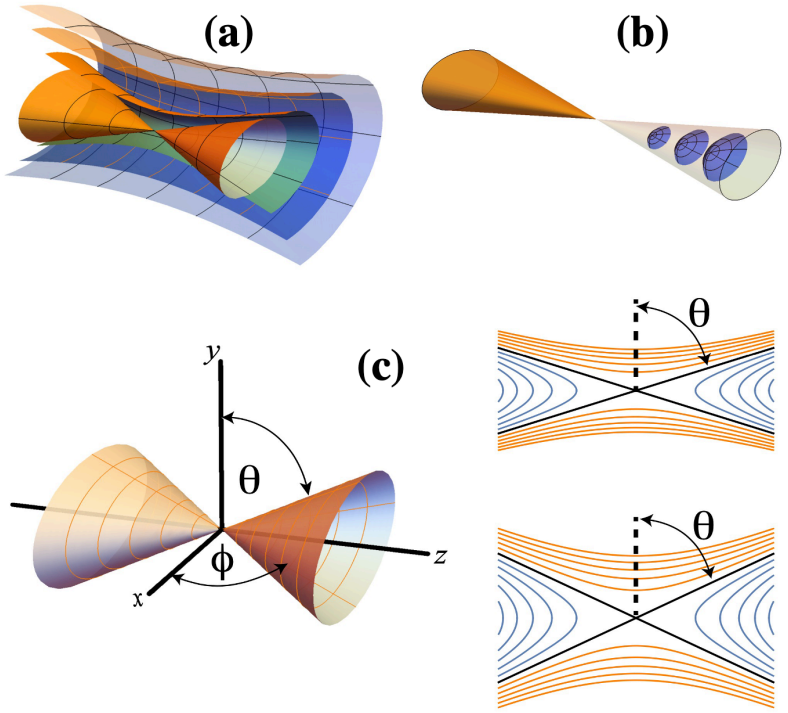

Figure 4. The isosurfaces near a bond CP. The isosurface passing through the bond CP will have the form of an elliptic cone, with the bond path coincident with its axis. This cone is the asymptotic boundary separating the exterior isosurfaces (a) from those interior to the cone (b). (c) Exterior characteristic angles, θ and ϕ. As the angle θ decreases the hyperbolic region (orange) becomes more curved, while the convex region contours (blue) become less curved. Adapted with permission from Ref. 49.

Changes to a molecule's external potential due to any perturbation (molecular vibrations, applied fields, substitutions) will necessarily alter isosurface curvature. Note that this statement is key to relating what follows to our central goal of determining the effects of mid- and long-range environment on enzymatic catalysis. However, the extent of these alterations must be consistent with the requirement that the total Gaussian curvature of any simple closed surface is 4π. Thus, for example, perturbations that increase the saddle character of a surface must be offset by regions on the surface where convexity increases. As it is common to picture the charge density in a plane as a series of contours, it is useful for illustrative purposes to generalize to closed curves. In this case, regardless of its shape, the integrated curvature around a closed contour line will be 2.

In addition to the geometric constraints acting on individual isosurfaces and contours, the form of the charge density imposes constraints on the character of nested isosurfaces. These effects are most obvious near a bond CP. To briefly explain: To second order the shape of the charge density around a bond CP can be written as,[26,46,47]

$$\rho(r) - \rho_{bcp} = \frac{1}{2}\left(\rho_{zz}z^2 - \rho_{xx}x^2 - \rho_{yy}y^2\right). \qquad (1)$$

where the bond CP serves as the origin; ρ_{bcp} is the value of the charge density at the bond CP; x, y and z are the eigenvectors of the Hessian of $\rho(\boldsymbol{r})$ at the bond CP and ρ_{xx}, ρ_{yy} and ρ_{zz} are the magnitudes of the corresponding eigenvalues, *e.g.*, $\rho_{xx} = |\frac{\partial^2\rho(r)}{\partial x^2}|$. We take z to be the direction parallel to the internuclear axis and hence ρ_{zz} is the positive eigenvalue while x and y are the directions of the negative eigenvalues.

When $\rho(\boldsymbol{r}) - \rho_{bcp}$ is positive, Equation 1 represents nested hyperboloids of two sheets (Figure 4b). When it is negative, it is the equation for nested hyperboloids of one sheet (Figure 4a). And when $\rho(\boldsymbol{r}) - \rho_{bcp} = 0$ (the isosurface passing through the bond CP, which has been previously recognized as chemically significant),[46,47] it is the equation for a double elliptic cone to which the two sets of hyperboloids are asymptotic (Figure 4c, left).

The cone passing through the bond CP is fully characterized by its two exterior angles θ and ϕ (Figure 4c, left), with $\tan(\theta) = \sqrt{\frac{\rho_{yy}}{\rho_{zz}}}$ and $\tan(\phi) = \sqrt{\frac{\rho_{xx}}{\rho_{zz}}}$. For a fixed value of ρ_{bcp} the curvatures of the isosurfaces exterior to the cone are mediated by these angles, a perturbation that decreases $\frac{\rho_{yy}}{\rho_{zz}}$ and/or $\frac{\rho_{xx}}{\rho_{zz}}$ will necessarily change the curvature of these isosurfaces (Figure 4c, right).

As we are interested in the curvature of isosurfaces and contours, Equation (1) can be manipulated to give the curvature of the contours at their vertices (typically points of maximum absolute curvature) along the *x*, *y*, and *z* directions close to the bond CP. The vertex curvature of the internal contours along the *z* direction, denoted $\kappa_I(z)$, is given as:

$$\kappa_I(z) = \tan^2(\phi)\sqrt{\frac{\rho_{zz}}{2|\rho(z)-\rho_{bcp}|}} \qquad (2)$$

And the vertex curvature of the external contours along the *x* direction, denoted $\kappa_E(x)$, is given as:

$$\kappa_E(x) = \tan^{-1}(\phi)\sqrt{\frac{\rho_{zz}}{2|\rho(x)-\rho_{bcp}|}} \qquad (3)$$

With a similar set of equations for the vertex curvature of contours in the *yz* plane.

To illustrate the content behind Equations 2 and 3 we will draw from a set of calculations modelling vibrational effects in nine carbonyl containing molecules with varying compositions and subject to fields applied both parallel and antiparallel to the C=O bond path. The intent of these calculations is to predict field and composition effects on charge density geometries and vibrational frequencies. While the full results of these calculations will be discussed in another paper, our approach and findings to date can be illuminated by analyzing the results of the calculations on acetone (see Figure 5). Acetone with its C_{2v} symmetry facilitates a graphical interpretation of our results while still being relevant to many cases of enzymatic catalysis where carbonyl activation is critical (e.g., KSI, HDAC8, peptidases, etc.).

Figure 5 depicts the charge density in the *xz* mirror plane and their variation resulting from shortening the C=O distance by 1.5%. As expected, the isosurface variations are most apparent in the interatomic region where the perturbation energy from the bond shortening is comparable to the local potential. Near the nuclei, where the coulomb potential is very large compared to the perturbation energy, isosurface deviations are small, and close to the nucleus virtually imperceptible. However, near acetone's C=O BCP the contour deviation is apparent and depicted in the explode views of Figure 5.

We begin our analysis with equilibrium field free acetone. Figure 5a shows two internal and external contours "close" to the C=O BCP. The vertices of these contours are marked with small cyan and orange spheres respectively. An increase in the $\rho(\boldsymbol{r})$ difference in Equations 2 and 3, which occurs as we move farther from the BCP, results in a proportionate decrease in instantaneous curvature.

As suggested by Figure 4c, Equations 2 and 3 confirm that, in the absence of changes to ρ_{bcp}, increasing the exterior angle ϕ will increase the curvature of internal contours (making them more positive) and

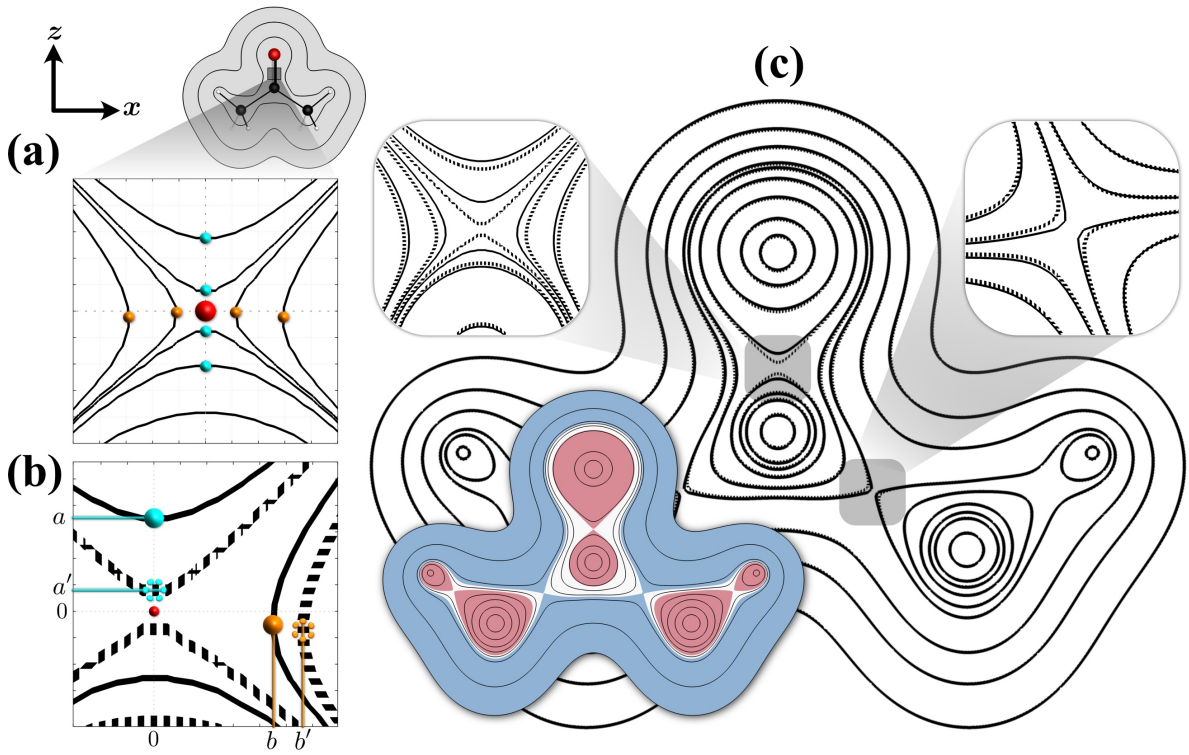

Figure 5. (a) Contours of $\rho(\boldsymbol{r})$ in acetone near to the C=O bond critical point (red), with internal (cyan) and external (orange) vertices indicated. (b,c) Solid contours are those of relaxed acetone while dashed contours are those of acetone with a 1.5% compression of the C=O bond but otherwise relaxed. The dashed-solid contour pairs are defined by the same $\rho(\boldsymbol{r})$ values; they show how the contour moved in response to the compression. (b) The internal (a; cyan) and external (b; orange) vertices are indicated. *a'* and *b'* indicate the same vertices for the C=O compressed system. (c) Corresponding contours of $\rho(\boldsymbol{r})$ near the C=O bond CP (top-left) and C–C bond CP (top-right); the inset indicates the first, second, and third classes of contours in relaxed acetone with red, white, and blue shading respectively.

decrease the curvature of external contours (making them less negative). The extent of the variations will be scaled by changes in the magnitude of ρ_{zz}.

Similarly, a perturbation that alters the density at the BCP while holding the θ and ϕ constant, will have opposite effects on the internal and external vertex curvatures. Take an internal contour whose vertex is a distance a from the BCP (Figure 5b; cyan). Since this is an internal contour, $\rho(a) > \rho_{bcp}$, a perturbation that increases the density at the BCP must decrease $|\rho(a) - \rho_{bcp}|$ and hence increase the vertex curvature of this contour, which will necessitate the movement of the contour vertex toward the BCP to a new location, a'. Note that the contour value does not change, only the shape of the contour is altered. For an external contour whose vertex is a distance b from the bond CP, $\rho(b) < \rho_{bcp}$. A perturbation that increases the density at the bond CP must increase $|\rho(b) - \rho_{bcp}|$ and hence decrease the vertex curvature of this contour, which will be accompanied by the movement of the contour vertex further from the bond CP to b' (Figure 5b; orange).

The key concept here is that the response of the charge density to perturbations is correlated over finite regions—changes at one point in such regions necessitate geometrically required responses at other points.

3.2. Vibrations and charge density geometry

We can bring these principles together to explore the global response of the charge density to vibrations and the effect of applied electric fields to these vibrations. Note that the C=O stretch of an activated carbonyl in enzymes such as KSI is a key vibration aligned with the reaction coordinate. If this vibration is promoted to be less harmonic, the barrier to the reaction will decrease. The argument in the field therefore centers on how vibrations such as this, *i.e.* important for crossing the reaction barrier, are affected by the protein scaffold. The PPV theory states that the protein dynamics flatten the relevant modes and thus promote the reaction.[8,23,48] We note that an electric field experienced by the active site due to the presence of the protein scaffold is tightly linked to the configuration and motion of the protein. Furthermore, an applied field can cause mode flattening, and so can cause a geometric change. An applied field must affect vibrations, and the field experienced by the activated molecule is affected by the configurational change to the active site due to protein dynamics. In other words, the two phenomena, often placed in opposition to each other, are one and the same. As a proof of that, we show in this section how the vibrational motion (which can be PPV) and an applied field (which can come from the protein scaffold) cause identical perturbations to the charge density, and therefore, inescapably, correlate with the barrier change via the identical quantum mechanical process.

Here we will simulate the changes to the geometry of the charge density through the carbonyl stretch of acetone, both in the absence and presence of an EEF applied parallel to the C=O bond and known to activate the carbonyl O.[35,37,49] The charge redistribution associated with the C=O stretch of acetone was simulated by first employing ADF[c,50,51] to determine the equilibrium geometry of acetone, yielding a C=O bond distance of 122.5 pm. Subsequently, the C=O distance was compressed by 1.5% and held fixed while all other atoms were allowed to relax to their minimum energy configuration. A second pair of calculations was performed, this time with a rather large electric field—on the order of those measured in KSI via vibrational Stark spectroscopy—of 100 MV/cm applied parallel to the C=O axis and pointing from the O to the C atom. In the presence of this field the entire molecule was allowed to relax to an equilibrium geometry giving a C=O bond distance of 124.3 pm. A vibration in the presence of the field was again simulated by compressing the C=O distance by 1.5% while allowing all other atoms to relax.[d]

The compression of 1.5% was chosen as a sensible room temperature vibrational amplitude as determined for organic molecules from Debye-Waller factors. Further with this magnitude, the energy of a C=O stretch was calculated to be of the order of 0.01 eV and so will occur with reasonable frequency at room temperature. Finally, this vibrational amplitude is of the same order as the field induced relaxations of the C=O bond distance, putting comparison of the field and vibration induced perturbations on the same footing. Table 1 provides a summary of important parameters resulting from these calculations.

Figures 5b and 5c depict superimposed contours in acetone's molecular plane. Solid contours are those of equilibrium acetone and the dashed contours are those of acetone with the constrained C=O bond distance—the perturbed system. The contours for both systems are characterized by the same values of charge density. The same visual analysis was performed for acetone in the presence of an applied EEF, and the C=O compression-induced charge redistribution (depicted in the right inset of Figure 6) is indiscernible from that absent the EEF.

---

[c] The calculations employed ADF's "normal" numerical quality, a TZP basis set, and the GGA:PBE density functional.

[d] The same set of calculations has been performed on all nine molecules of our larger set. In addition, we also stretched the C=O distance by 1.5% to simulate the full vibration. The acetone results we discuss here are illustrative of the results from the larger set of calculations.

For acetone, the C=O bond CP exterior angles θ (in the *xz-plane)* and ϕ (Figure 4) are respectively 40.6° and 39.3°. For the perturbed system the values diminish slightly to 39.4° and 38.1°. However, the effect of the perturbation on ρ_{bcp} and ρ_{zz} are more influential to the contour curvatures, with an increase of nearly 4% and 17% respectively. As discussed, and as is evident in Figure 5, the flow of density to the region around the C=O bond CP, scaled by the change to ρ_{zz}, increases the curvature of internal contours and flattens the curvature of the external contours.

This effect is most apparent in the region adjacent to the C=O bond critical point and becomes less significant for contours more distant from this CP. In Figure 5, this is evidenced by greater separation between the solid and dashed contour pairs close to the bond CP that decreases precipitously for contour pairs farther from the bond CP. Consistent with the vibration induced accumulation of density around the bond CP, these changes to isosurface curvature cause high value contours to expand, displacing lower value contours. We define these deviations as positive and note that the region over which a perturbation induces positive contour deviation will, through the perturbation, attract electron density. The opposite effect, where high value contours contract, we define as negative contour deviation and charge density will be depleted or donated over regions where a perturbation induces negative contour deviation. Obviously, for any process, regions of positive and negative contour deviation must be coupled. By this, we mean that regions which are strongly coupled will experience greater charge redistribution in response to the same nuclear motion than regions that are weakly coupled. This leads to a similar picture to that of electron pushing arrows, where arrow width would indicate coupling strength. The mechanism responsible for this coupling is based on geometric principles.

Because changes to isosurface or contour curvature must produce corresponding changes elsewhere on the isosurface or contour, these variations effectively couple distant regions of the molecule. For illustration, we identify 3 classes of contours in Figure 5c based on the number CPs interior to each. In the first class (red) are contours that are interior to the C=O and C–H bond isosurfaces. These contours fully enclose one atomic nuclear CP (O, C or H). In class 2 (white) are contours that are exterior to the C=O or C–H bond isosurfaces but interior to the C–C bond isosurface. These contours encircle C and O (or C and H) nuclear CPs. Finally, in class three (blue) are contours external to the C=O, C–C, and C–H bond isosurfaces. For acetone, these contours lie on isosurfaces to which all the molecule's nuclear CPs are interior.

Beginning with the first contour class, the increased curvature of these contours near the C=O bond-point mandates that there be a decrease of contour curvature at some other location around the contour. Inspection of Figure 5c reveals this occurs along the points of the contour most distant from the C=O bond CP (red-shaded regions). That is, the points adjacent and distant from the C=O bond CP are geometrically linked and undergo perturbation-induced compensatory intra-atomic charge redistribution.

More interesting from our perspective is the second class of contours. The shortening of the C–O distance has caused these contours to become less negatively curved near the C=O bond CP. The loss of negative curvature requires a corresponding loss of positive curvature (or a gain in negative curvature) elsewhere in order that the total curvature around the contour be 2π. This response is most profound near the C–C bond isosurface where the interior contours become less curved, indicative of charge transfer from the region about the C–C bond CP into the region about C=O bond CP. We recognize this response as an inductive effect where the donation or withdraw of density from one region of a molecule—the C=O bonding region—is facilitated by the withdrawal or donation of density through connected σ-bonds—the neighboring C–C bonding region. We believe that the conservation of curvature about contours is the geometrically required basis for inductive effects.

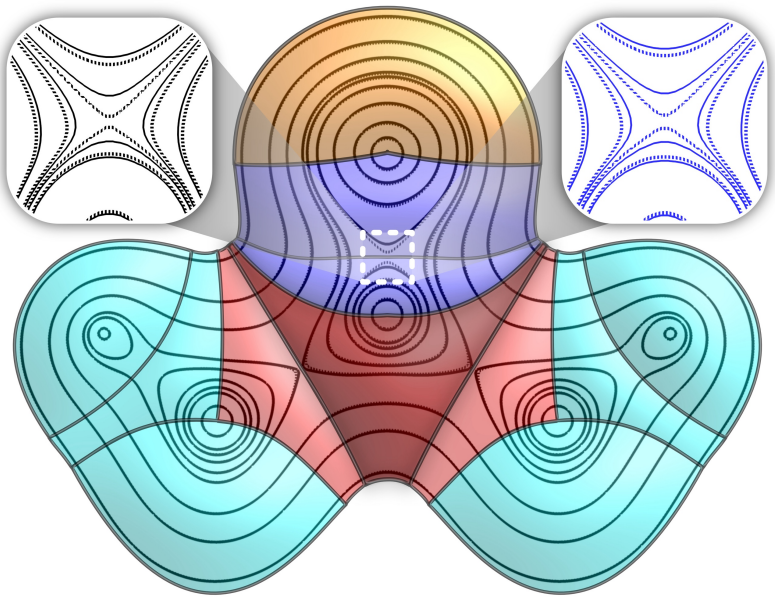

Figure 6. Contours of $\rho(\boldsymbol{r})$ in acetone (solid) and in acetone with a 1.5% C=O bond compression (dashed). Bond bundle and lone pair bundle boundaries coincide with those separating regions of positive and negative contour deviation. The insets show a zoomed image of the C=O bond CP region (left) as well as the same region in the EEF system (right; blue contours). The blue solid-dashed contour pairs correspond to a different set of $\rho(\boldsymbol{r})$ values chosen to match black contours relative to bond and nuclear CPs.

Finally, the vibration couples the charge density of the third class of contours over comparatively large distances. The flattening of the contours external to both the C=O and C–C bond CPs necessitates an increase of curvature elsewhere on these contours. Inspection of Figure 5 shows this occurs over the lone pair region of the carbonyl O atom and on the distal end of the H atoms located in the molecular plane. The correlated response of the charge density over these distant atomic basins is again a geometric requirement for points that sit on a common isosurface.

Returning to the coupling produced by the contours of the first and second classes, we have marked the boundaries separating the regions of positive and negative contour deviation around the C=O and C–C bond CPs. In these mirror planes, these regions, as determined by inspection, lie very close or coincide with what are called bond bundles (BBs) and are shown schematically in Figure 6.[52–56] In an arbitrary plane, these regions may or may not coincide with bond-bundle boundaries, but our preliminary calculations suggest for small perturbations to the charge density isosurfaces the boundaries separating regions of compensatory charge redistribution are well approximated by bond bundle boundaries.

Like atomic basins, BBs are characterized by well-defined energies and other properties, such as each contains a specific number of electrons. BBs are intrinsic to a molecule and not determined by the perturbation. It is noteworthy, however, that the boundaries of the BBs of Figure 6 are coincident, or nearly coincident, with the boundaries separating regions of positive and negative contour deviation.

Four BB are depicted in Figure 6: *i*) The orange lone pair BB over which contour deviation is negative; *ii*) The blue C=O BB characterized by positive deviation; *iii*) The red C–C BBs over which the contour deviation is predominantly negative; and *iv*) The cyan C–H BBs in which there is little—though not zero—contour deviation. There is a further partitioning of BBs into what are called bond wedges. These are the intersection of a BB with the atomic basins of the bound atoms. Conceptually they are that part of a bond "belonging" to each of the bound atoms. Attention is drawn to the bond wedges of the C–C BB,

which are portrayed with different shades of red, with the darker bond wedge being that part of the C–C bond belonging to the C atom of the carbonyl.

The characteristic vibrational frequency of a carbonyl stretch is around 1700 cm^{-1}. However, changes to the substituent attached to the α-C can alter this value by as much as ± 75 cm^{-1}. We hypothesize that these shifts are determined by the extent of geometrically required vibrational induced coupling to the region of contour deviation around the C=O bond CP, *i.e.* the C=O BB. For acetone the region of greatest compensatory contour deviation is found around the C–C BB, and the larger part of this deviation is confined to the bond wedge of the carbonyl C. Hence, we expect that the coupling of charge redistribution between the C=O BB and the bond wedge of the carbonyl C–C BB to have the greatest effect on the C=O stretch frequency. We hypothesize that perturbations that increase the coupling between these two regions will decrease the C=O stretch frequency by facilitating the charge redistribution inherent to the vibration.[47]

We may test this hypothesis by using the Bondalyzer package[57,58] to integrate the density contained in the bond wedges of Figure 6 and compute the coupling between these two regions for acetone with and without an EEF and comparing these values to the respective calculated vibrational frequencies. The calculated C=O stretch frequency of acetone is 1711 cm^{-1}. The same vibration in the presence of our field is calculated to be 1644 cm^{-1}. Table 1 gives the relative changes to the charge density contained in the C=O BB (blue) and carbonyl C–C bond wedges due to the simulated vibration for both the reference acetone and field perturbed acetone.

In the absence of a field, the simulated C=O stretch increases the number of electrons in the C=O bond bundle by 0.85% while decreasing those in the carbonyl C–C bond wedge by 0.32%. With the EEF, the number of electrons transferred to C=O BB increases in both absolute numbers and as a percentage to 1.85%, while the number of electrons in the carbonyl C–C bond wedge decreases by 0.46%. Apparently,

			Acetone NEF			Acetone EEF		
	property		Equil.	C=O comp.	Δ%	Equil.	C=O comp.	Δ%
C=O bond	stretch freq. [cm^{-1}]		1711			1644		
	distance [pm]		122.5	120.69	-1.48	124.3	122.4	-1.53
	Bond CP	$\rho(r_{bcp})$	0.3996	0.4148	3.80	0.3813	0.397	4.12
		ρ_{zz}	1.378	1.6117	16.96	1.217	1.4452	18.75
		ρ_{xx}	-1.014	-1.0867	7.17	-0.883	-0.9533	7.96
		ρ_{yy}	-0.922	-0.9906	7.44	-0.939	-1.0116	7.73
		θ [degrees]	40.6	39.4	-2.96	40.4	39.1	-3.22
		φ [degrees]	39.3	38.1	-3.05	41.3	39.9	-3.39
	bond bundle ρ [e]		**3.664**	**3.695**	**0.85**	**3.403**	**3.466**	**1.85**
C–C bond CP	$\rho(r_{bcp})$		0.2445	0.243	-0.61	0.2504	0.2494	-0.40
	$\rho_{bond\ axis}$		0.4092	0.4096	0.10	0.4079	0.4086	0.17
	$\rho_{mol.\ plane}$		-0.477	-0.4735	-0.73	-0.4929	-0.4905	-0.49
	ρ_{yy}		-0.4567	-0.4533	-0.74	-0.4681	-0.4658	-0.49
	θ [degrees]		47.2	47.1	-0.21	47.7	47.6	-0.21
	φ [degrees]		46.6	46.5	-0.21	47.0	46.9	-0.21
Carbonyl C: C–C bond wedge ρ [e]			**1.868**	**1.862**	**-0.32**	**1.963**	**1.954**	**-0.46**

Table 1. Geometric bond and bond CP properties for the C=O and C–C bonds in acetone. Atomic units are used where not indicated. The regional electron counts are included for the C=O bond bundle and the bond wedge of the carbonyl C corresponding to the C–C bond.

the field enhances the compensatory charge redistribution between the C=O BB and the carbonyl C–C bond wedge. Plainly stated, these two regions are more strongly coupled by the applied electric field.

We conclude that for this toy problem, the field known to activate the O atom of the carbonyl simultaneously softens the C=O stretch frequency. Both responses are due to the same effect—the field induced coupling between the carbonyl C–C bond wedge and the C=O BB. It seems that O activation and lowering the C=O stretch frequency are different aspects of the same phenomenon—the geometrically constrained redistribution of charge density.

4. Summary

In summary, the numerous hypotheses put forward for the role that the protein plays in enzymatic catalysis (e.g., active site rigidification, PPV, electrostatic preorganization) are linked, and ultimately affect the electronic structure of the reactant, in such a way that the reaction coordinate mode flattens, and the barrier is reduced. All these phenomena can be unified. The quantum mechanical electron density portrait of reactant activation looks the same, whether it is painted by vibrations, or by applied fields. In addition, vibrations and fields are connected because fields are produced by atomic configurations, and in turn affect atomic motion, as a chicken and an egg. In this article, we propose a way to rigorously assess the effect of the protein on the catalyzed reaction.

The fundamentals unifying the response of the charge density to perturbative influences, whether from vibrations or electric fields, are rooted in geometric principles—the conservation of isosurface Gaussian curvature. This fact implicates isosurface curvature as a parameter constraining charge redistribution. Curvature conservation connects regions involved in what we think of as charge transfer. It places limits on where we can draw the heads and tails of our curvy arrows. While we laid out the geometric principles mediating charge redistribution using a model system, these principles are quite general and apply to any molecular system regardless of its complexity. And as we have demonstrated,[59] with computational methods able to isolate and integrate over region of characteristic isosurface curvature, these principles can provide insight into the response of the charge density at one point in an enzyme brought about by changes at a distant location.

Using these tools in our future work, we are excited to address the dynamics of the active site charge density. The charge density will fluctuate in the course of thermal protein dynamics, and given the correlation of the geometry of ρ and reactivity, it is interesting to know whether the best performing enzymes exhibit minimal fluctuations (*i.e.* the active site is strictly preorganized), or fluctuations that allow the reactants most frequent visits to highly reactive configurations of the charge density. Natural and directed evolution lineages of enzymes are under our current investigation. We also suggest that geometries of charge density in the active site are conserved within large enzyme classes, even if individual proteins in the class differ dramatically in sequence and molecular weight. This conjecture is based on our studies of classical electric fields at enzyme active sites. For example, Fe-heme proteins going through the Fe(IV)=O intermediate exhibit fields at Fe produced by the protein scaffold (except for the heme and the axial ligand) that are highly correlated with their function.[60] The strongest field opposing the Fe(IV)=O bond increases the radical character of the oxygen, and is present in oxidases, which are Cys ligated. These proteins can activate strong C–H bonds. Nearly zero fields at the Fe are characteristic of Tyr-ligated catalases, and fields pointing from Fe to O are characteristic of His-ligated peroxidases. A Fe-heme site (with the axial ligand) placed in a foreign field is predicted to gain an adverse or unnatural function. In blue Cu proteins, the fields are uniform across the entire class, the facilitate the kick-off of a ligand, needed for the redox function in these electron transport proteins.[61] Therefore, we must also see strong similarities of charge density across a variety of enzyme classes.

The direction for our theoretical work is motivated by these observations and the need to provide a more rigorous link between electric fields and charge density geometry. While the overall effect of an electric field on the charge density must preserve curvature, the specifics of this response require further investigation. Why, for example, do we observe that the perturbative effect of a field seems to be most pronounced at points of maximum isosurface curvature? We would like to better understand the chemistry and perhaps geometry that drives this response. Clearly, there is much left to be discovered regarding in the relationships between charge density geometry and enzyme function.

Acknowledgements

This work was supported by the NSF CHE grant 2203366, ONR 558 grant N00014-05-C-0241, and by the State of Colorado AIA 2021 grant. Computational resources were provided by XSEDE.

References

(1) Warshel, A.; Sharma, P. K.; Kato, M.; Xiang, Y.; Liu, H.; Olsson, M. H. M. Electrostatic Basis for Enzyme Catalysis. *Chem. Rev.* **2006**, *106* (8), 3210–3235. https://doi.org/10.1021/cr0503106.

(2) Warshel, A. Electrostatic Origin of the Catalytic Power of Enzymes and the Role of Preorganized Active Sites*. *J. Biol. Chem.* **1998**, *273* (42), 27035–27038. https://doi.org/10.1074/jbc.273.42.27035.

(3) Schneider, S. H.; Boxer, S. G. Vibrational Stark Effects of Carbonyl Probes Applied to Reinterpret IR and Raman Data for Enzyme Inhibitors in Terms of Electric Fields at the Active Site. *J. Phys. Chem. B* **2016**, *120* (36), 9672–9684. https://doi.org/10.1021/acs.jpcb.6b08133.

(4) Weaver, J. B.; Kozuch, J.; Kirsh, J. M.; Boxer, S. G. Nitrile Infrared Intensities Characterize Electric Fields and Hydrogen Bonding in Protic, Aprotic, and Protein Environments. *J. Am. Chem. Soc.* **2022**, *144* (17), 7562–7567. https://doi.org/10.1021/jacs.2c00675.

(5) Fried, S. D.; Bagchi, S.; Boxer, S. G. Extreme Electric Fields Power Catalysis in the Active Site of Ketosteroid Isomerase. *Science* **2014**, *346* (6216), 1510–1514.

(6) Wu, Y.; Boxer, S. G. A Critical Test of the Electrostatic Contribution to Catalysis with Noncanonical Amino Acids in Ketosteroid Isomerase. *J. Am. Chem. Soc.* **2016**, *138* (36), 11890–11895. https://doi.org/10.1021/jacs.6b06843.

(7) Schneider, S. H.; Kozuch, J.; Boxer, S. G. The Interplay of Electrostatics and Chemical Positioning in the Evolution of Antibiotic Resistance in TEM β-Lactamases. *ACS Cent. Sci.* **2021**, *7* (12), 1996–2008. https://doi.org/10.1021/acscentsci.1c00880.

(8) Schramm, V. L.; Schwartz, S. D. Promoting Vibrations and the Function of Enzymes. Emerging Theoretical and Experimental Convergence. *Biochemistry* **2018**, *57* (24), 3299–3308. https://doi.org/10.1021/acs.biochem.8b00201.

(9) Basner, J. E.; Schwartz, S. D. How Enzyme Dynamics Helps Catalyze a Reaction in Atomic Detail: A Transition Path Sampling Study. *J. Am. Chem. Soc.* **2005**, *127* (40), 13822–13831. https://doi.org/10.1021/ja043320h.

(10) Antoniou, D.; Schwartz, S. D. Protein Dynamics and Enzymatic Chemical Barrier Passage. *J. Phys. Chem. B* **2011**, *115* (51), 15147–15158. https://doi.org/10.1021/jp207876k.

(11) Silva, R. G.; Murkin, A. S.; Schramm, V. L. Femtosecond Dynamics Coupled to Chemical Barrier Crossing in a Born-Oppenheimer Enzyme. *Proc. Natl. Acad. Sci.* **2011**, *108* (46), 18661–18665. https://doi.org/10.1073/pnas.1114900108.

(12) Núñez, S.; Antoniou, D.; Schramm, V. L.; Schwartz, S. D. Promoting Vibrations in Human Purine Nucleoside Phosphorylase. A Molecular Dynamics and Hybrid Quantum Mechanical/Molecular Mechanical Study. *J. Am. Chem. Soc.* **2004**, *126* (48), 15720–15729. https://doi.org/10.1021/ja0457563.

(13) Suarez, J.; Schramm, V. L. Isotope-Specific and Amino Acid-Specific Heavy Atom Substitutions Alter Barrier Crossing in Human Purine Nucleoside Phosphorylase. *Proc. Natl. Acad. Sci.* **2015**, *112* (36), 11247–11251. https://doi.org/10.1073/pnas.1513956112.

(14) Davarifar, A.; Antoniou, D.; Schwartz, S. D. The Promoting Vibration in Human Heart Lactate Dehydrogenase Is a Preferred Vibrational Channel. *J. Phys. Chem. B* **2011**, *115* (51), 15439–15444. https://doi.org/10.1021/jp210347h.

(15) Dametto, M.; Antoniou, D.; Schwartz, S. D. Barrier Crossing in Dihydrofolate Reductase Does Not Involve a Rate-Promoting Vibration. *Mol. Phys.* **2012**, *110* (9–10), 531–536. https://doi.org/10.1080/00268976.2012.655337.

(16) Masterson, J. E.; Schwartz, S. D. Evolution Alters the Enzymatic Reaction Coordinate of Dihydrofolate Reductase. *J. Phys. Chem. B* **2015**, *119* (3), 989–996. https://doi.org/10.1021/jp506373q.

(17) Layfield, J. P.; Hammes-Schiffer, S. Calculation of Vibrational Shifts of Nitrile Probes in the Active Site of Ketosteroid Isomerase upon Ligand Binding. *J. Am. Chem. Soc.* **2013**, *135* (2), 717–725. https://doi.org/10.1021/ja3084384.

(18) Liu, C. T.; Layfield, J. P.; Stewart, R. J. I.; French, J. B.; Hanoian, P.; Asbury, J. B.; Hammes-Schiffer, S.; Benkovic, S. J. Probing the Electrostatics of Active Site Microenvironments along the Catalytic Cycle for Escherichia Coli Dihydrofolate Reductase. *J. Am. Chem. Soc.* **2014**, *136* (29), 10349–10360. https://doi.org/10.1021/ja5038947.

(19) Bradshaw, R. T.; Dziedzic, J.; Skylaris, C.-K.; Essex, J. W. The Role of Electrostatics in Enzymes: Do Biomolecular Force Fields Reflect Protein Electric Fields? *J. Chem. Inf. Model.* **2020**, *60* (6), 3131–3144. https://doi.org/10.1021/acs.jcim.0c00217.

(20) Bhowmick, A.; Sharma, S. C.; Head-Gordon, T. The Importance of the Scaffold for de Novo Enzymes: A Case Study with Kemp Eliminase. *J. Am. Chem. Soc.* **2017**, *139* (16), 5793–5800. https://doi.org/10.1021/jacs.6b12265.

(21) Kamerlin, S. C. L.; Warshel, A. The Empirical Valence Bond Model: Theory and Applications. *WIREs Comput. Mol. Sci.* **2011**, *1* (1), 30–45. https://doi.org/10.1002/wcms.10.

(22) Kamerlin, S. C. L.; Sharma, P. K.; Chu, Z. T.; Warshel, A. Ketosteroid Isomerase Provides Further Support for the Idea That Enzymes Work by Electrostatic Preorganization. *Proc. Natl. Acad. Sci.* **2010**, *107* (9), 4075–4080. https://doi.org/10.1073/pnas.0914579107.

(23) Chalopin, Y. The Physical Origin of Rate Promoting Vibrations in Enzymes Revealed by Structural Rigidity. *Sci. Rep.* **2020**, *10* (1), 17465. https://doi.org/10.1038/s41598-020-74439-5.

(24) Welborn, V. V.; Head-Gordon, T. Fluctuations of Electric Fields in the Active Site of the Enzyme Ketosteroid Isomerase. *J. Am. Chem. Soc.* **2019**, *141* (32), 12487–12492. https://doi.org/10.1021/jacs.9b05323.

(25) Zoi, I.; Antoniou, D.; Schwartz, S. D. Electric Fields and Fast Protein Dynamics in Enzymes. *J. Phys. Chem. Lett.* **2017**, *8* (24), 6165–6170. https://doi.org/10.1021/acs.jpclett.7b02989.

(26) Bader, R. F. W. *Atoms in Molecules: A Quantum Theory*; Clarendon Press: Oxford, 1990.

(27) Matta, C. F.; Boyd, R. J. *The Quantum Theory of Atoms in Molecules: From Solid State to DNA and Drug Design*; Weinheim: Wiley-VCH, 2007.

(28) Popelier, P. L. A. *Atoms in Molecules: An Introduction*; Prentice Hall: Harlow, 2000.

(29) Nasertayoob, P.; Shahbazian, S. Revisiting the Foundations of the Quantum Theory of Atoms in Molecules: Toward a Rigorous Definition of Topological Atoms. *Int. J. Quantum Chem.* **2009**, *109* (4), 726–732. https://doi.org/10.1002/qua.21864.

(30) Heidarzadeh, F.; Shahbazian, S. The Quantum Divided Basins: A New Class of Quantum Subsystems. *Int. J. Quantum Chem.* **2011**, *111* (12), 2788–2801. https://doi.org/10.1002/qua.22629.

(31) Morgenstern, A.; Jaszai, M.; E. Eberhart, M.; N. Alexandrova, A. Quantified Electrostatic Preorganization in Enzymes Using the Geometry of the Electron Charge Density. *Chem. Sci.* **2017**, *8* (7), 5010–5018. https://doi.org/10.1039/C7SC01301A.

(32) Kraut, D. A.; Sigala, P. A.; Pybus, B.; Liu, C. W.; Ringe, D.; Petsko, G. A.; Herschlag, D. Testing Electrostatic Complementarity in Enzyme Catalysis: Hydrogen Bonding in the Ketosteroid Isomerase Oxyanion Hole. *PLOS Biol.* **2006**, *4* (4), e99. https://doi.org/10.1371/journal.pbio.0040099.

(33) Herschlag, D.; Natarajan, A. Fundamental Challenges in Mechanistic Enzymology: Progress toward Understanding the Rate Enhancements of Enzymes. *Biochemistry* **2013**, *52* (12), 2050–2067. https://doi.org/10.1021/bi4000113.

(34) Warshel, A.; Sharma, P. K.; Chu, Z. T.; Åqvist, J. Electrostatic Contributions to Binding of Transition State Analogues Can Be Very Different from the Corresponding Contributions to Catalysis: Phenolates Binding to the Oxyanion Hole of Ketosteroid Isomerase. *Biochemistry* **2007**, *46* (6), 1466–1476. https://doi.org/10.1021/bi061752u.

(35) Hennefarth, M. R.; Alexandrova, A. N. Direct Look at the Electric Field in Ketosteroid Isomerase and Its Variants. *ACS Catal.* **2020**, *10* (17), 9915–9924. https://doi.org/10.1021/acscatal.0c02795.

(36) Fuller, J.; Wilson, T. R.; Eberhart, M. E.; Alexandrova, A. N. Charge Density in Enzyme Active Site as a Descriptor of Electrostatic Preorganization. *J. Chem. Inf. Model.* **2019**, *59* (5), 2367–2373. https://doi.org/10.1021/acs.jcim.8b00958.

(37) Hennefarth, M. R.; Alexandrova, A. N. Heterogeneous Intramolecular Electric Field as a Descriptor of Diels–Alder Reactivity. *J. Phys. Chem. A* **2021**, *125* (5), 1289–1298. https://doi.org/10.1021/acs.jpca.1c00181.

(38) Hennefarth, M. R.; Alexandrova, A. N. Advances in Optimizing Enzyme Electrostatic Preorganization. *Curr. Opin. Struct. Biol.* **2022**, *72*, 1–8. https://doi.org/10.1016/j.sbi.2021.06.006.

(39) Meir, R.; Chen, H.; Lai, W.; Shaik, S. Oriented Electric Fields Accelerate Diels–Alder Reactions and Control the Endo/Exo Selectivity. *ChemPhysChem* **2010**, *11* (1), 301–310. https://doi.org/10.1002/cphc.200900848.

(40) Shaik, S.; Danovich, D.; Dubey, K. D.; Stuyver, T. The Impact of Electric Fields on Chemical Structure and Reactivity. In *Effects of Electric Fields on Structure and Reactivity*; The Royal Society of Chemistry, 2021; pp 12–70. https://doi.org/10.1039/9781839163043-00012.

(41) Aragonès, A. C.; Haworth, N. L.; Darwish, N.; Ciampi, S.; Bloomfield, N. J.; Wallace, G. G.; Diez-Perez, I.; Coote, M. L. Electrostatic Catalysis of a Diels–Alder Reaction. *Nature* **2016**, *531* (7592), 88–91. https://doi.org/10.1038/nature16989.

(42) Preiswerk, N.; Beck, T.; Schulz, J. D.; Milovník, P.; Mayer, C.; Siegel, J. B.; Baker, D.; Hilvert, D. Impact of Scaffold Rigidity on the Design and Evolution of an Artificial Diels-Alderase. *Proc. Natl. Acad. Sci.* **2014**, *111* (22), 8013–8018. https://doi.org/10.1073/pnas.1401073111.

(43) Siegel, J. B.; Zanghellini, A.; Lovick, H. M.; Kiss, G.; Lambert, A. R.; St.Clair, J. L.; Gallaher, J. L.; Hilvert, D.; Gelb, M. H.; Stoddard, B. L.; Houk, K. N.; Michael, F. E.; Baker, D. Computational Design of an Enzyme Catalyst for a Stereoselective Bimolecular Diels-Alder Reaction. *Science* **2010**, *329* (5989), 309–313.

(44) Vaissier Welborn, V.; Head-Gordon, T. Computational Design of Synthetic Enzymes. *Chem. Rev.* **2019**, *119* (11), 6613–6630. https://doi.org/10.1021/acs.chemrev.8b00399.

(45) Vargas, S.; Hennefarth, M. R.; Liu, Z.; Alexandrova, A. N. Machine Learning to Predict Diels–Alder Reaction Barriers from the Reactant State Electron Density. *J. Chem. Theory Comput.* **2021**, *17* (10), 6203–6213. https://doi.org/10.1021/acs.jctc.1c00623.

(46) Eberhart, M. E. The Metallic Bond: Elastic Properties. *Acta Mater.* **1996**, *44* (6), 2495–2504.

(47) Eberhart, M. E.; Jones, T. E. Cauchy Pressure and the Generalized Bonding Model for Nonmagnetic Bcc Transition Metals. *Phys. Rev. B* **2012**, *86* (13), 134106. https://doi.org/10.1103/PhysRevB.86.134106.

(48) Wang, Z.; Chang, E. P.; Schramm, V. L. Triple Isotope Effects Support Concerted Hydride and Proton Transfer and Promoting Vibrations in Human Heart Lactate Dehydrogenase. *J. Am. Chem. Soc.* **2016**, *138* (45), 15004–15010. https://doi.org/10.1021/jacs.6b09049.

(49) Wilson, T. R.; Alexandrova, A. N.; Eberhart, M. E. Electron Density Geometry and the Quantum Theory of Atoms in Molecules. *J. Phys. Chem. A* **2021**, *125* (50), 10622–10631. https://doi.org/10.1021/acs.jpca.1c09359.

(50) Baerends, E. J.; Ziegler, T.; Atkins, A. J.; Autschbach, J.; Bashford, D.; Baseggio, O.; Bérces, A.; Bickelhaupt, F. M.; Bo, C.; Boerritger, P. M.; Cavallo, L.; Daul, C.; Chong, D. P.; Chulhai, D. V.; Deng, L.; Dickson, R. M.; Dieterich, J. M.; Ellis, D. E.; van Faassen, M.; Ghysels, A.; Giammona, A.; van Gisbergen, S. J. A.; Goez, A.; Götz, A. W.; Gusarov, S.; Harris, F. E.; van den Hoek, P.; Hu, Z.; Jacob, C. R.; Jacobsen, H.; Jensen, L.; Joubert, L.; Kaminski, J. W.; van Kessel, G.; König, C.; Kootstra, F.; Kovalenko, A.; Krykunov, M.; van Lenthe, E.; McCormack, D. A.; Michalak, A.; Mitoraj, M.; Morton, S. M.; Neugebauer, J.; Nicu, V. P.; Noodleman, L.; Osinga, V. P.; Patchkovskii, S.; Pavanello, M.; Peeples, C. A.; Philipsen, P. H. T.; Post, D.; Pye, C. C.; Ramanantoanina, H.; Ramos, P.; Ravenek, W.; Rodŕiguez, J. I.; Ros, P.; Rüger, R.; Schipper, P. R. T.; Schlüns, D.; van Schoot, H.; Schreckenbach, G.; Seldenthuis, J. S.; Seth, M.; Snijders, J. G.; Solà, M.; M., S.; Swart, M.; Swerhone, D.; te Velde, G.; Tognetti, V.; Vernooijs, P.; Versluis, L.; Visscher, L.; Visser, O.; Wang, F.; Wesolowski, T. A.; van Wezenbeek, E. M.; Wiesenekker, G.; Wolff, S. K.; Woo, T. K.; Yakovlev, A. L. ADF2019, SCM, Theoretical Chemistry, Vrije Universiteit, Amsterdam, The Netherlands. *ADF* **2019**.

(51) te Velde, G.; Bickelhaupt, F. M.; Baerends, E. J.; Fonseca Guerra, C.; van Gisbergen, S. J. A.; Snijders, J. G.; Ziegler, T. Chemistry with ADF. *J. Comput. Chem.* **2001**, *22* (9), 931–967. https://doi.org/10.1002/jcc.1056.

(52) Morgenstern, A.; Wilson, T.; Miorelli, J.; Jones, T.; Eberhart, M. E. In Search of an Intrinsic Chemical Bond. *Comput. Theor. Chem.* **2015**, *1053* (0), 31–37. http://dx.doi.org/10.1016/j.comptc.2014.10.009.

(53) Morgenstern, A.; Eberhart, M. Bond Dissociation Energies from the Topology of the Charge Density Using Gradient Bundle Analysis. *Phys. Scr.* **2016**, *91* (2), 23012.

(54) Morgenstern, A.; Morgenstern, C.; Miorelli, J.; Eberhart, M. E.; Wilson, T. The Influence of Zero-Flux Surface Motion on Chemical Reactivity. *Phys. Scr.* **2016**, *18* (7), 5638–5646. https://doi.org/10.1039/C5CP07852K.

(55) Wilson, T. R.; Eberhart, M. E. Quantum Theory of Atoms in Molecules in Condensed Charge Density Space. *Can. J. Chem.* **2019**, *97* (11), 757–762. https://doi.org/10.1139/cjc-2019-0086.

(56) Wilson, T.; Eberhart, M. A Bond Bundle Case Study of Diels-Alder Catalysis Using Oriented Electric Fields. In *Advances in Quantum Chemical Topology Beyond QTAIM, Chapter 17*; Rodríguez, J. I., Guzman, F., Anderson, J. S. M., Eds.; Elsevier: Netherlands, 2022.

(57) Wilson, T. R.; Eberhart, M. E. *Bondalyzer*. Bondalyzer (https://github.com/moltheorygroup/BondalyzerTecplotAddon). https://github.com/moltheorygroup/BondalyzerTecplotAddon (accessed 2022-09-27).

(58) Tecplot Inc. *Tecplot 360 2013R1*. Tecplot 360 2013R1 (https://www.tecplot.com). https://www.tecplot.com.

(59) Wilson, T. R.; Morgenstern, A.; Alexandrova, A. N.; Eberhart, M. E. Bond Bundle Analysis of Ketosteroid Isomerase. *J. Phys. Chem. B* **2022**. https://doi.org/10.1021/acs.jpcb.2c03638.

(60) Bím, D.; Alexandrova, A. N. Local Electric Fields As a Natural Switch of Heme-Iron Protein Reactivity. *ACS Catal*. **2021**, *11* (11), 6534–6546. https://doi.org/10.1021/acscatal.1c00687.

(61) Bím, D.; Alexandrova, A. N. Electrostatic Regulation of Blue Copper Sites. *Chem. Sci*. **2021**, *12* (34), 11406–11413. https://doi.org/10.1039/D1SC02233D.